Regular Article

PHYSICAL CHEMISTRY RESEARCH
Published by the
Iranian Chemical Society
www.physchemres.org
info@physchemres.org

Phys. Chem. Res., Vol. 12, No. 2, 273-287, June 2024
DOI: 10.22036/pcr.2023.377475.2258

Construction of ZnS/montmorillonite/graphitic Carbon Nitride as Adsorbent and Photocatalyst for the Removal of Rhodamine B

M. Chegeni* and F. Nasrollahi

Department of Chemistry, Faculty of Basic Science, Ayatollah Boroujerdi University, Boroujerd, Iran

(Received 21 December 2022, Accepted 29 July 2023)

In this work, the ZnS/montmorillonite/graphitic carbon nitride (ZnS/MMT/g-C_3N_4) as a novel composite was synthesized through a simple strategy. The addition of MMT showed positive impact on increasing the specific surface area of g-C_3N_4, and the photocatalytic activity of g-C_3N_4 was improved by using ZnS as a semiconductor. We used several techniques including X-ray powder diffraction, Fourier transform infrared spectroscopy, Field emission scanning electron microscopy, energy-dispersive X-ray spectroscopy, Ultraviolet-visible light diffuse reflectance spectroscopy, Brunauer-Emmett-Teller analysis, high-resolution transmission electron microscopy, and photoluminescence spectroscopy were used to confirm the formation of the as-synthesized composite. The adsorption and photocatalytic activities of ZnS/MMT/g-C_3N_4 were evaluated to examine its ability for the removal of Rhodamine B (Rh. B). Response surface methodology was used to study the important parameters and their interaction in the adsorption process. The pH, adsorbent dose, and dye concentration were effect factors on the adsorption process, and the adsorption process was corresponded to Freundlich isotherm and pseudo-second-order kinetic models. The photocatalytic activity of ZnS/MMT/g-C_3N_4 was studied under several condition, and the best result was 93% yield under ultra violet irradiation. This study presents a novel adsorbent and photocatalyst composite with high yield for the removal of Rh. B dye.

Keywords: Montmorillonite, Graphitic carbon nitride, Photocatalyst, Adsorbent

INTRODUCTION

Today, the energy and environmental subjects are studied by many scientists, and the dispel of environmental problems is an important issue. Hence, the exploitation of novel, ecofriendly, and appropriate compounds is considered in environmental subjects. In recent years, carbon nitride compound was studied by several researchers due to its extraordinary properties. Todays, g-C_3N_4 is applied as photocatalyst [1], biosensor [2], bionanocomposite [2], and water splitting [1]. G-C_3N_4 as an old polymer can be synthesized by earth-abundant elements including carbon and nitrogen atoms, which can be modulated by surface chemistry. The π-conjugated electronic structure of g-C_3N_4 can be limited by low surface and recombination of charge carriers [1].

In the view of surface and textural, bulk g-C_3N_4 is modified by several strategies including change of crystal structure and the formation of nano and hetero structures [3]. In single-phase compounds, the problems of g-C_3N_4 properties were remained, but the synthesis of g-C_3N_4-based heterostructure as a suitable strategy has been considered in the reported literatures such as cobalt-doped graphitic carbon nitride [4], graphitic carbon nitride-alumina [5], graphitic-carbon nitride based mixed-phase bismuth [6], carbon nitride stabilized FeS [7], copper sulfide-titania-graphitic carbon nitride [8], and 1D SWCNT/2D ultrathin C_3N_4 [9].

In recent years, the use of natural materials such as kaolinite [10], illite [10], perlite [11], bauxite [12], and bentonite [13] was extended for the development of g-C_3N_4

*Corresponding author. E-mail: mahdieh.chegeni@abru.ac.ir

application. Montmorillonite (MMT) as a natural clay belongs to the smectite group, which includes O-Si-O and O-Al (Mg)-O with layer structure (two tetrahedral silica sheets and an octahedral alumina sheet). MMT is used in pharmacology, electrochemical sensor [14], asphalt material [15], and an adsorbent for organic molecules and heavy metals [16]. There are many research reporting the use of MMT for the formation of composites such as polypropylene/MMT [17], HDPE/MMT-based [18], WS_2/montmorillonite [19], nafion/sulfonated montmorillonite [20], and $MoSe_2$/Montmorillonite [21].

On the other hand, Zinc sulfide (ZnS) as a semiconductor is extensively used in optical device due to its band gap, ecofriendly, suitable physical property, and low-cost. Indeed, ZnS can be combined with other materials for being used in novel application. Numerous studies reported ZnS-based composite such as ZnS@graphite [22], NiS@ZnS [23], Ag_2S/ZnS [24], and ZnO/ZnS [25].

The removal of hazardous materials such as dyes and organic pollutant is an important aim of green chemistry. Various strategies were studied for the dyes removal using chemical precipitation [26], conventional coagulation [27], electrolysis [28], reverse osmosis [29], ion-exchange [30], adsorption [31], electrodialysis [32], enzymatic hydrolysis [33], biological treatment [34], and photocatalytic process [35]. Some of these methods showed low yield, difficult procedure, by product formation, and expensive equipment. A few of these processes could remove pollutant between the phases, and the main pollutant was remained in the media. Among these methods, photocatalytic reaction has been reported as a low cost, easy operation, and reliable procedure for the decrease of wastewater treatment. One of the important ways in water purification is using semiconductor photocatalyst, by which the pollutants can be decomposed to fewer toxic materials such as CO_2 and H_2O with low energy. So, the design of a novel photocatalyst is an interesting subject, which can show bifunction application including adsorption and photocatalysis activities [36].

Based on the appropriate adsorption capacity, low-cost, and ecofriendly characters of MMT, it was used for the modification of g-C_3N_4 properties. The ZnS was applied to improve the photocatalytic property of g-C_3N_4. ZnS/montmorillonite/graphitic carbon nitride (ZnS/MMT/g-C_3N_4), which was synthesized through a simple procedure and characterized by several techniques such as X-ray diffraction (XRD), Fourier transform infrared spectroscopy (FTIR), field emission scanning electron microscopy (FESEM), energy-dispersive X-ray spectroscopy (EDX), ultraviolet-visible light diffuse reflectance spectra (UV-DRS), Brunauer-Emmett-Teller (BET) analysis, high-resolution transmission electron microscopy (HRTEM), and photoluminescence (PL) spectroscopy. The as-synthesized composite was used to study the dye removal by adsorption and photocatalytic procedures. The Rhodamine B (Rh. B, *N*-[9(ortho-carboxyphenyl)-6-(diethylamino)-3*H*-xanthen-3-ylidene] diethyl ammonium chloride) was considered as a pigment, which its harmful effect is known in the industrial wastewater [37].

In the environmental studies, response surface methodology (RSM) has been used as an optimized tool to design some empirical models, decreasing the cost and time of experiments. The central composite design (CCD) model is a useful method for the optimization of variables and responses. The adsorption activity of ZnS/MMT/g-C_3N_4 was evaluated by using RSM-CCD design, and pH, adsorbent doses, Rh. B concentration, time, and temperature were determined. Then, the photocatalytic degradation of Rh. B was studied at optimum condition under various irradiations by using ZnS/MMT/g-C_3N_4.

MATERIALS AND METHODS

Melamine, Montmorillonite, Zinc sulfide (ZnS), hydrochloric acid (HCl, 0.1 M), and Sodium hydroxide (NaOH, 0.1 M) were purchased from Merck and Aldrich companies. The functional groups were determined by Unicam-Galaxy 5000 with KBr pellets, and the information of morphology was used by field emission scanning electron microscopy (FESEM, TescanMira3-Lmu), and high-resolution transmission electron microscopy (HRTEM, FEI, TEC9G20, USA). The crystal phase of compounds was obtained by Panalytical Xpertpro diffractometer Cu Kα radiation (λ = 1.54178 Å). The electronic property was evaluated by UV-Vis diffuse reflectance spectroscopy (DRS, Unicam UV-Vis spectrophotometer), and photoluminescence (PL, PerkinElmer LS-55 fluorescence Spectrometer) spectra. The Rh. B concentration was obtained by Dynamica-HALO- DB–20, Germany.

Synthesis of ZnS/MMT/g-C_3N_4

First, 1.5 g of montmorillonite was mixed with 60 ml distillated water for 30 min at 70 °C, then 1 g melamine was added for 60 min at 70 °C. Then, the mixture was filtrated and heated in crucible for 90 min at 550 °C, and ZnS was mixed with MMT/g-C_3N_4 at the ratio of 0.8:1. The mixture was heated for 2 h at 90 °C to obtain ZnS/MMT/g-C_3N_4 composite.

RSM Method

Experimental design was done by RSM method as a mathematical method, which contains advantages including low cost, which can determine the effective parameters and their interactions. Central composite design (CCD) was used as a based method of RSM to obtain synergic factor towards by designing 50 experiments for various pH, Rh. B concentration, adsorbent dose, time, and temperature. The independent variables were coded at -1 and +1 as low and high levels by using Design-Expert 13.0 (Tables 1, 2). The pHpzc (point of zero charge) was determined as 7.8, the net charge of adsorbent surface was zero, and experiments were carried out based on the CCD-design. The mixture was at equilibrium condition, and the solution was filtrated and centrifuged. Then, the adsorbed dye concentration was determined by UV-visible spectrophotometer at 561 nm. The important parameterS such as removal percentage (Re) (%) and Q_e were obtained based on the Eqs. ((1) and (2)).

$$\text{Removal}\ (\%) = \frac{C_i - C_e}{C_i} * 100 \quad (1)$$

$$Q_e = \frac{(C_i - C_e) * V}{M} \quad (2)$$

C_i: the intial concentration,
C_e: the equbiliruim concentration,
Q_e: the Rh. B concentration adsorbed at the equilibrium $\left(\frac{\text{mg}}{\text{g}}\right)$,
C_i: the Rh. B concentration (mg l^{-1}),
Ce: the Rh. B Equilibrium concentration (mg l^{-1}),
$V =$ Volume (l), M: the adsobent mass (g)

Adsorption Isotherms and Kinetics Studies

To identify the adsorption process, the Freundlich and Langmuir isotherms were studied as two well-known models. The Eqs. ((3) and (4)) are explained multilayer (Freundlich) and monolayer adsorption (Langmuir). The kinetic adsorption is evaluated by the pseudo-first-order and pseudo-second-order kinetic models, which are shown by Eqs. ((5), and (6)).

$$lnq_e = lnk_f + \left(\frac{1}{n}\right) \ln C_e \quad (3)$$

$$\frac{C_e}{q_e} = \frac{1}{bq_m} + \frac{C_e}{q_m} \quad (4)$$

$$\log(q_e - q_t) = logq_e - \frac{K_l}{2.303}\, t \quad (5)$$

$$\frac{t}{q_t} = \frac{1}{K_2\, q_e^2} + \frac{t}{q_e} \quad (6)$$

In above equations, q_e is the equilibrium adsorption capacity (mg g^{-1}); K_F and n are the model constants displaying the relationship between adsorption capacity and adsorption intensity; C_e is the equilibrium concentration solution (mg l^{-1}); b is the Langmuir isotherm constant (l mg^{-1}); q_m is the maximum monolayer adsorption capacity (mg g^{-1}); q_e and q_t are the adsorption amounts of Rh. B, adsorbed at equilibrium and at different times t (mg g^{-1}); K_l is : the rate constant; K_2 is also : the rate constant.

Photocatalytic Study

When the optimum conditions were obtained at the adsorption process, the photocatalytic degradation of Rh. B was studied under dark, light-emitting diode (LED, 5 W LED lamps, 450 nm, 2 cm distance from the sample), and ultraviolet (UV, 300 W Xe lamp, 345 nm cut off filter, 4 cm distance from the sample) irradiations condition.

RESULTS AND DISCUSSION

ZnS/MMT/g-C_3N_4 composite was prepared through thermal strategy, and various techniques were applied to confirm the formation of as-prepared composite. The functional groups were evidenced by using FTIR spectroscopy, which are shown in Fig. 1. The peak at 809 cm^{-1} is corresponded to the *s*-triazine unit, and the absorption peaks at 1237-1649 cm^{-1} are ascribed by CN heterocyclic compounds. The bands in the range of 3000-3330 cm^{-1} are belonged to hydroxyl, primary and secondary

Table 1. Experimental Factors and Levels for Rh. B Adsorption on ZnS/MMT/g-C_3N_4

Factor	Name	Units	Minimum	Maximum	Coded low	Coded high
A	pH		2.00	9.00	-1 ↔ 2.00	+1 ↔ 9.00
B	Adsorbent dose	g	0.0100	0.1000	-1 ↔ 0.01	+1 ↔ 0.10
C	Rh. B	ppm	2.00	8.00	-1 ↔ 2.00	+1 ↔ 8.00
D	Temp.	°C	15.00	45.00	-1 ↔ 15.00	+1 ↔ 45.00
E	Time	min	30.00	150.00	-1 ↔ 30.00	+1 ↔ 150.00

Table 2. Experimental Design for Five-level-five Factors CCD for Rh. B Adsorption on ZnS/MMT/g-C_3N_4

Run	A:pH	B:Adsorbent dose (g)	C:Rh.B (ppm)	D:Temp. (°C)	E:Time (min)
1	6	0.01	2	20	30
2	4	0.06	5	20	30
3	4	0.06	2	15	90
4	2	0.06	6	30	150
5	9	0.04	5	45	30
6	6	0.06	8	40	60
7	2	0.06	6	30	150
8	2	0.04	2	40	90
9	6	0.06	8	40	60
10	2	0.01	8	45	30
11	8	0.1	5	30	90
12	9	0.1	3	20	30
13	4	0.06	5	20	30
14	2	0.1	2	15	150
15	6	0.01	6	45	120
16	9	0.08	8	45	150
17	6	0.1	2	40	30
18	9	0.1	8	15	30
19	6	0.1	2	45	150
20	8	0.1	5	30	90
21	2	0.01	5	30	60
22	2	0.01	3	15	150
23	2	0.08	8	15	90
24	9	0.06	3	40	120
25	6	0.08	6	15	150
26	9	0.01	8	20	90
27	2	0.1	6	45	60
28	6	0.01	6	45	120
29	4	0.01	8	15	150
30	9	0.06	2	15	90
31	9	0.01	2	30	150

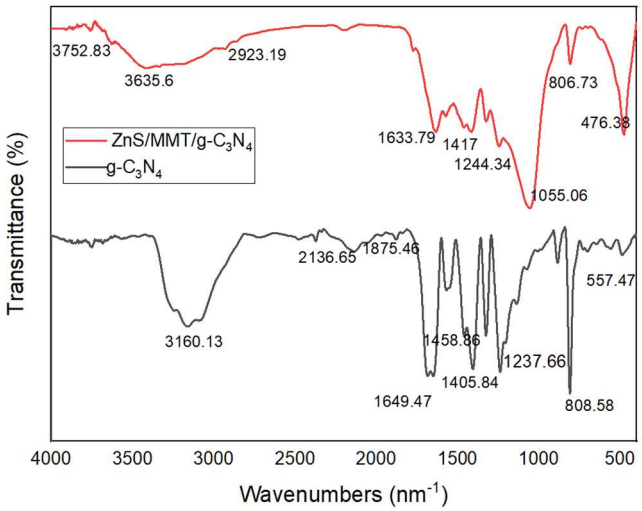

Fig. 1. FTIR spectra of g-C_3N_4 and ZnS/MMT/g-C_3N_4.

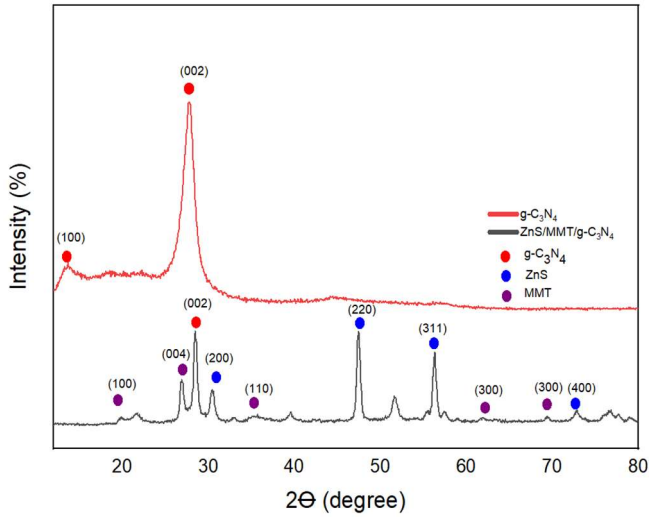

Fig. 2. XRD spectra of g-C_3N_4 and ZnS/MMT/g-C_3N_4.

amines. The FTIR spectrum of ZnS/MMT/g-C_3N_4 showed the peaks at 3400-3600 cm^{-1}, which indicate the -O-H bonds and H-bonding between components. Based on the bentonite category, the MMT peaks can be seen at 593 and 698 cm^{-1}, which are corresponded to Si-O and Al-Al-OH bonds. Furthermore, the peaks at 476 and 806 cm^{-1} are assigned by Zn-O and *s*-triazine bonds; the existence of main peaks can be explained by the formation of as-prepared composite.

Figure 2 shows the crystal structure of g-C_3N_4 and ZnS/MMT/g-C_3N_4 using X-ray powder diffraction spectra. In the spectrum of g-C_3N_4, the peaks at 2ɵ = 13.2° and 27.4° are corresponded to the (100) and (002) crystal faces, which assigned by *s*-triazine ring and conjugated aromatic ring. For ZnS/MMT/g-C_3N_4, the peaks at 2ɵ = 13.2° and 27.4° belong to the g-C_3N_4. The ZnS compound is determined by the peaks at 2ɵ = 30°, 48°, 52°, and 56° (JPCDS No. 89-2156). Furthermore, MMT compound is indexed by 2ɵ = 19.8° (100), 28.61° (004, quartz), 34.8° (110) and 69.4° (300), respectively.

The morphology of the g-C_3N_4 and ZnS/MMT/g-C_3N_4 was studied by FESEM technique, as shown in Fig. 3. The g-C_3N_4 was seen as a layered and tight layered (Figs. 3a,b); the images of ZnS/MMT/g-C_3N_4 were determined by the integrated MMT sheets and the ZnS small particles (Figs. 3c,d). In addition, the EDS images of ZnS/MMT/g-C_3N_4 are shown in Fig. 4, showing that the elemental mappings determine the homogeneous distribution of C, N, and Zn atoms without any impure elements.

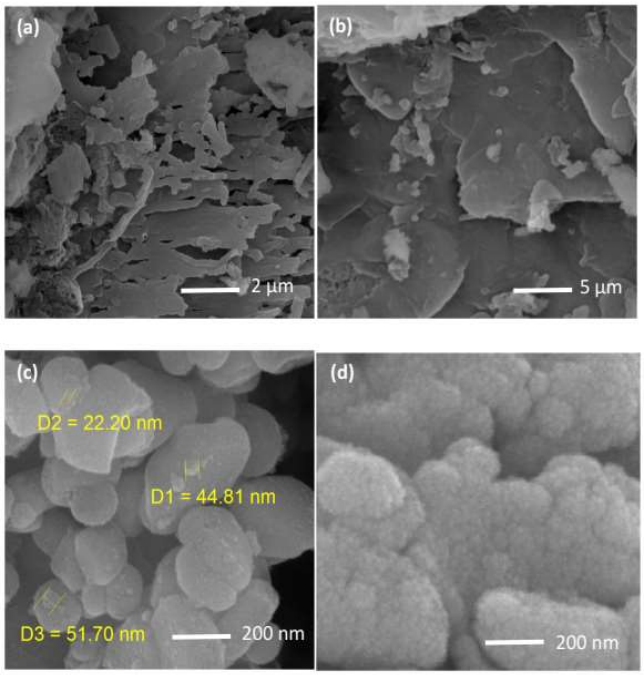

Fig. 3. FESEM images of (a,b) g-C_3N_4 and (c,d) ZnS/MMT/g-C_3N_4 composite.

The HRTEM images show the structure of ZnS/MMT/g-C_3N_4 composite, indicating that the ZnS particles spread on the MMT/g-C_3N_4 (Fig. 5) with d spacing of 3.5531.

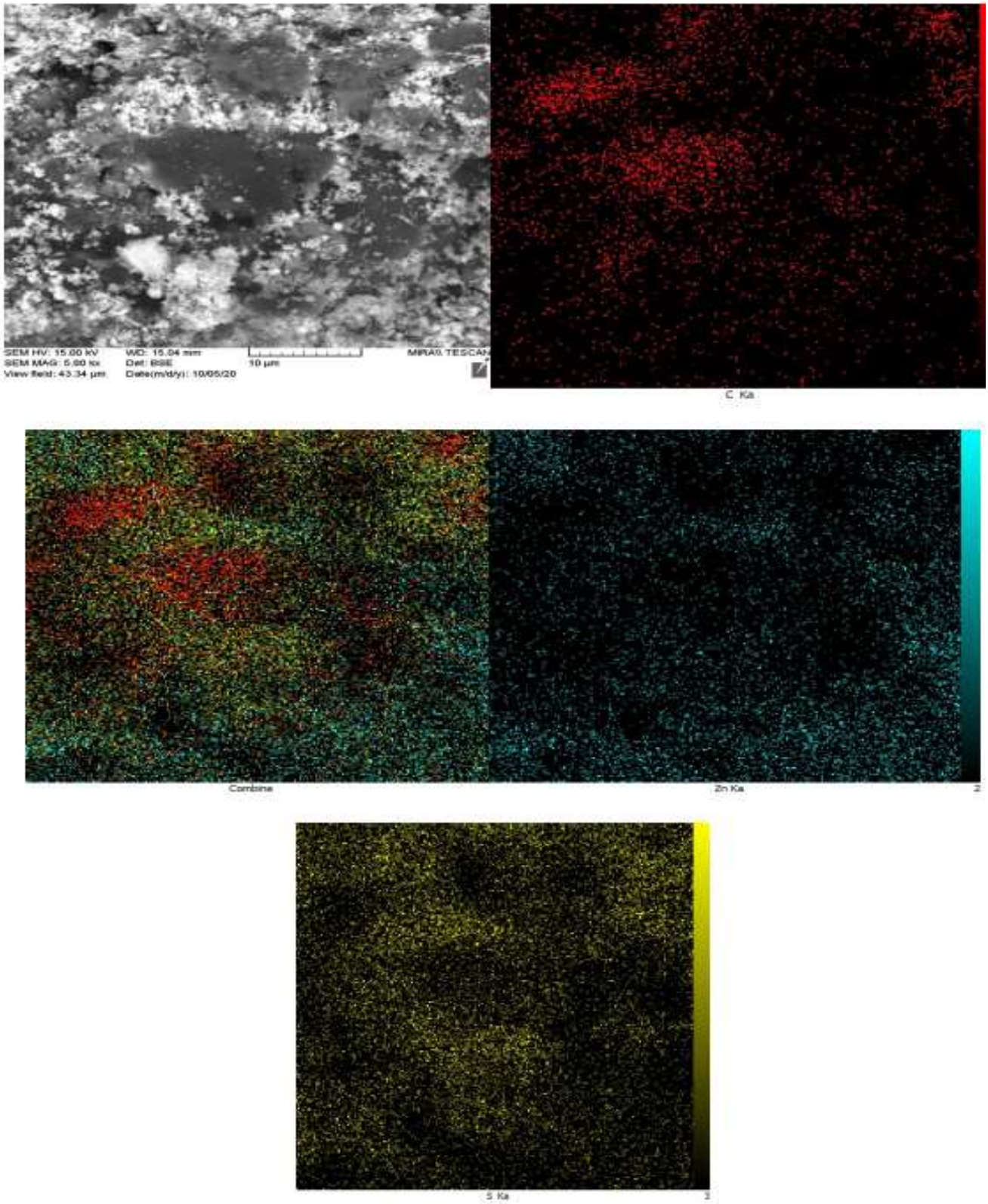

Fig. 4. EDX map of ZnS/MMT/g-C_3N_4 composite.

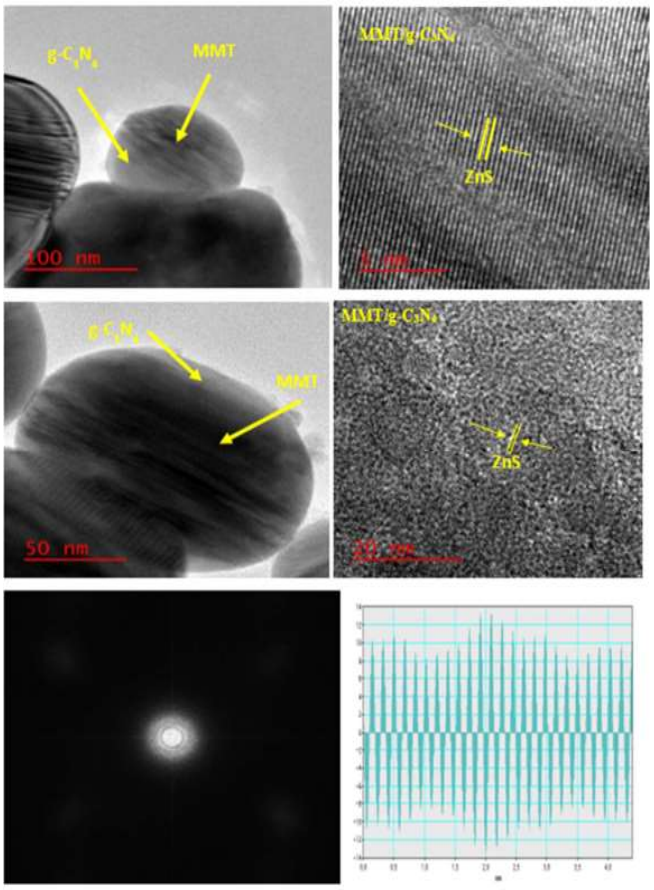

Fig. 5. HRTEM of ZnS/MMT/g-C_3N_4 composite.

The nitrogen adsorption-desorption isotherm was carried out to obtain the textural properties of the as-prepared composite. The BET specific area and the mean pore diameter of ZnS/MMT/g-C_3N_4 were 25.993 m^2 g^{-1} and 12.824 nm, showing higher amount compared to the pure g-C_3N_4 (13.47 m^2 g^{-1}), as shown in Fig. 6. Based on the results, the ZnS/MMT/g-C_3N_4 composite provided more adsorption and photocatalytic activities compared to those of g-C_3N_4. According to the IUPAC classification, the BET curves exhibited H3 hysteresis and type IV isotherms.

Also, photoluminescence spectra of g-C_3N_4 and ZnS/MMT/g-C_3N_4 are shown in Fig. 7. The higher photoluminescence peak shows the relatively faster charge recombination. The PL spectrum intensity of ZnS/MMT/g-C_3N_4 was lower than that of g-C_3N_4, which explaining the lower charge combination and good electrical conductivity of the as-prepared composite [38].

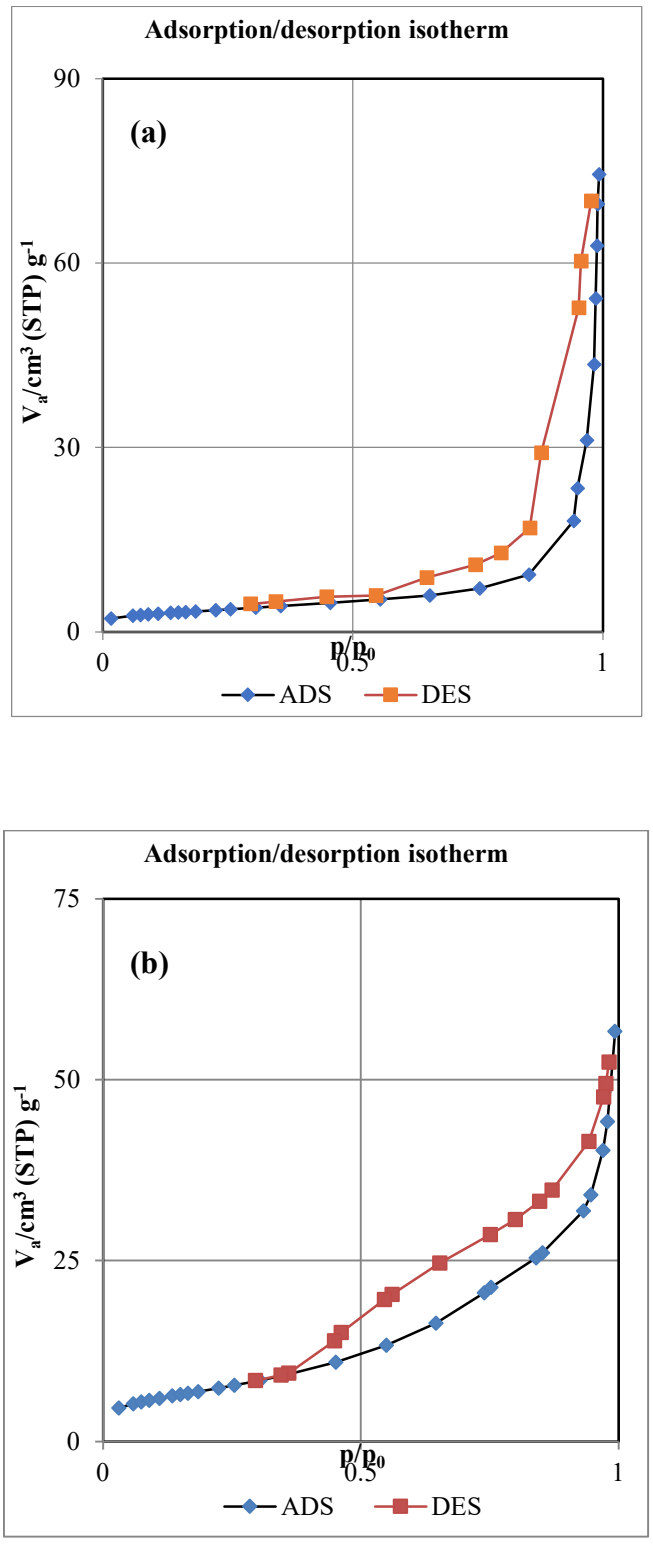

Fig. 6. N_2 adsorption-desorption curves of (a) g-C_3N_4, (b) ZnS/MMT/g-C_3N_4.

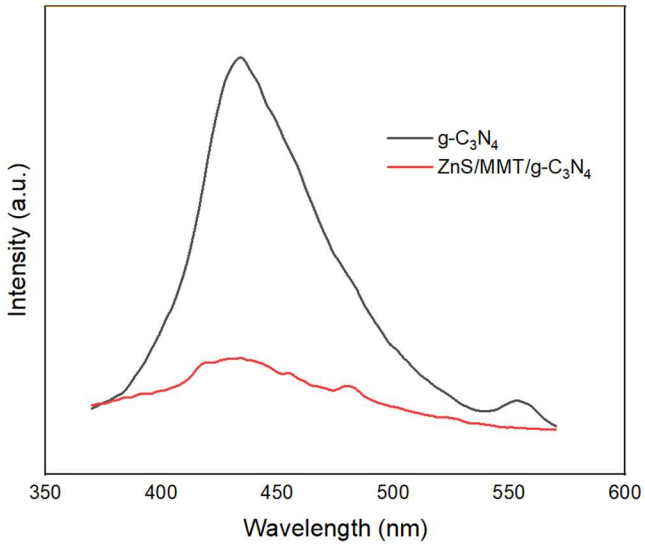

Fig. 7. PL spectra of g-C_3N_4 and ZnS/MMT/g-C_3N_4.

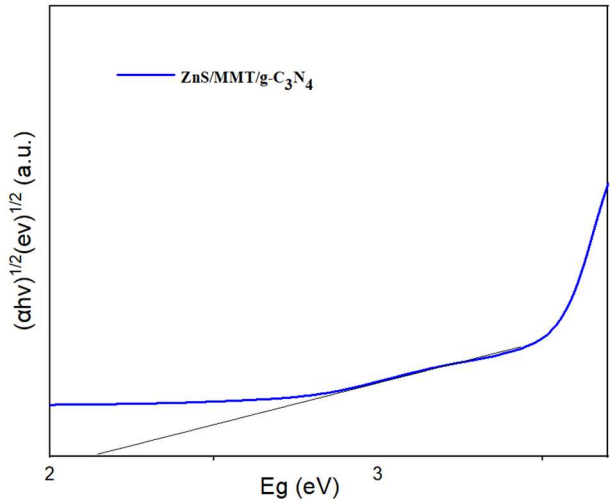

Fig. 8. UV-Vis diffuse reflectance curve of ZnS/MMT/g-C_3N_4.

The UV-Vis diffuse reflectance analysis was used to determine the optical absorption properties of ZnS/MMT/g-C_3N_4 (Fig. 8). The calculated band gap of as-prepared composite was 2.3 eV compared to g-C_3N_4 (2.58 eV), showing good potency for the photocatalytic activity.

Adsorption Study

The Rh. B adsorption on ZnS/MMT/g-C_3N_4 was studied by two-factor interactions (2FI), linear, quadratic, and cubic models based on CCD-RSM design. According to Table 3, the experimental data was fitted by a quadratic model, which the lack of Fit p-value > 0.2 and $R^2 > 0.95$.

Based on ANOVA analysis, the final Eq. (7) (in terms of actual factors) was constructed. In this equation, R^1 is the yield of Rh. B adsorption while A, B, and C terms are pH, adsorbent dose, and Rh. B concentration, respectively. According to the RSM results, D and E terms were shown less significant parameter compared to another parameters; hence, they were omitted from the ANOVA analysis. Synergic effects were described by negative and positive coefficient, which explain the increase of adsorbent dose resulted in high yield; the decrease of pH and Rh. B concentration led to high percentage adsorption.

$$R^1 = +106.71654-10.39655pH+1307.46315Adsorbent-5.04730Rh.B+60.10246pH*Adsorbent-9792.39589Adsorbent^2 \quad (7)$$

Contour plot explained the variables interaction and their effect. As shown in Fig. 9, the low pH and high adsorbent dose resulted in the high yield of Rh. B adsorption by using ZnS/MMT/g-C_3N_4. While the active sites of surface

Table 3. Model Summary Statistics

Source	Sequential p-value	Lack of Fit p-value	Adjusted R^2	Predicted R^2	
Linear	< 0.0001	0.0085	0.7283	0.6271	
2FI	0.3513	0.0080	0.7505	-0.0398	
Quadratic	0.0001	0.3355	0.9598	0.8041	Suggested
Cubic	0.3355		0.9678		Aliased

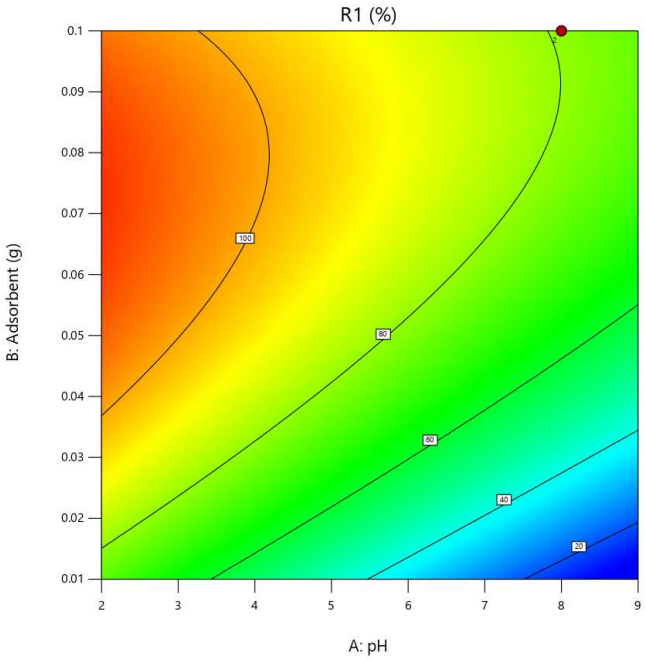

Fig. 9. Contour plot of the Rh. B removal.

were increased, the Rh. B adsorption was increased. Furthermore, the pHpz0 was 7.8, and the surface charge was positive at values less than 7.8, showing the interaction between Rh. B and ZnS/MMT/g-C_3N_4 had high percentage adsorption.

As represents in Fig. 10a, the residuals showed a good agreement between the experimental and predicted values, confirming the fitness of the selected model. The lack of clustering indicates the distribution of residuals. Based on the Fig. 10b, the 86.5 % yield of Rh. B adsorption was achieved at the optimum condition including pH of 5.5, 0.05 g ZnS/MMT/g-C_3N_4, 5 ppm Rh. B, 90 min, and 30 °C.

Isotherm Study

The relation between ZnS/MMT/g-C_3N_4 and Rh. B was studied by the Freundlich and Langmuir models. At the optimum condition, equilibrium adsorption isotherms were obtained (Fig. 11), and the Freundlich isotherm was related to the adsorption of Rh. B on ZnS/MMT/g-C_3N_4, due to the regression value ($R^2 = 0.98$, $n = 2.41$, $K_f = 0.1882$) compared to that of Langmuir isotherm ($R^2 = 0.96$). Based on the results, the π-π interaction resulted in the multilayer adsorption of Rh. B on the ZnS/MMT/g-C_3N_4.

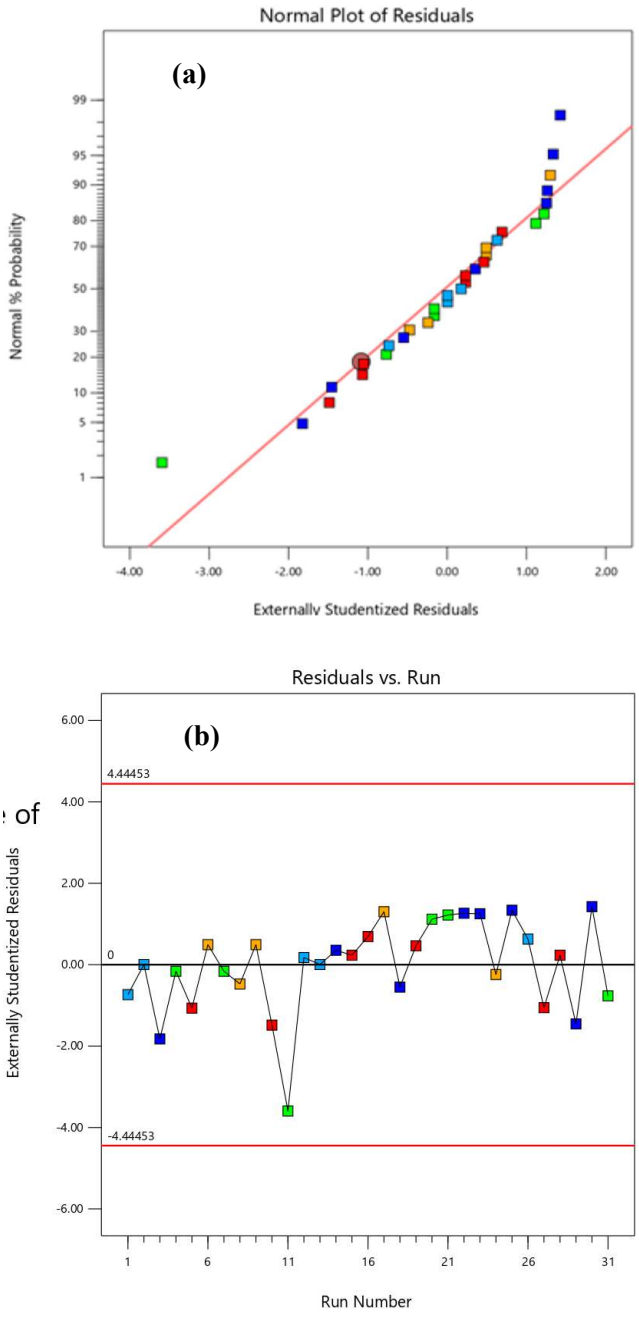

Fig. 10. RSM diagnostic plots for (a) Normal plot of residual, and (b) Residuals *vs*. Run for the Rh. B adsorption by ZnS/MMT/g-C_3N_4.

Adsorption Kinetic

The experimental data was evaluated with pseudo-first- and second-order kinetic models. According to Fig. 12, the

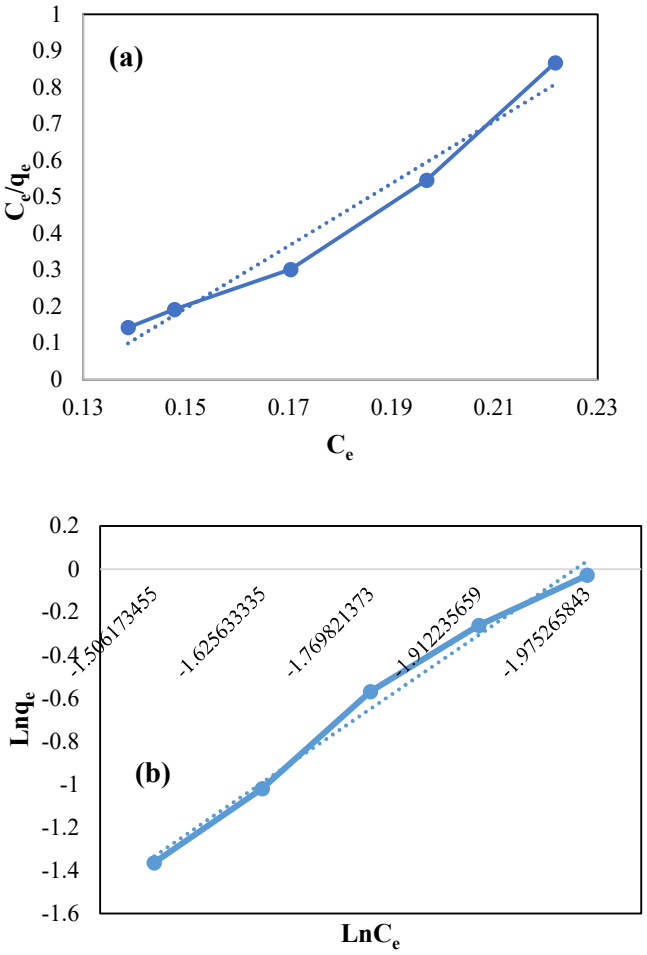

Fig. 11. (a) Langmuir isotherm and (b) Freundlich isotherm of Rh. B adsorption on ZnS/MMT/g-C_3N_4.

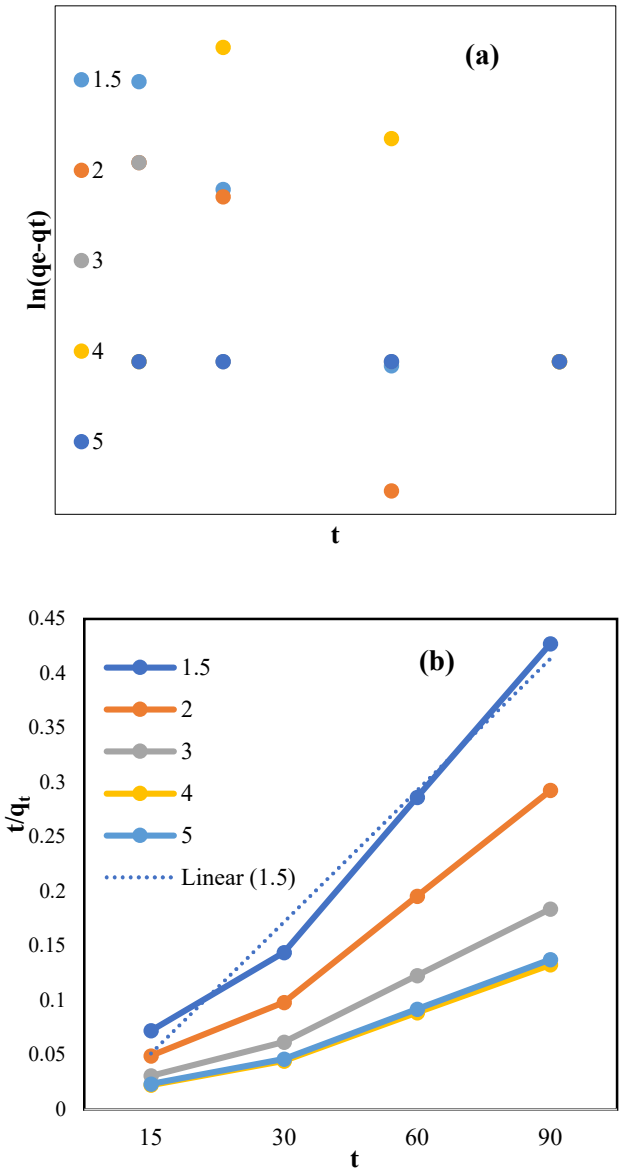

Fig. 12. (a) Pseudo-first-order kinetic, and (b) pseudo-second-order kinetic models for Rh. B removal by ZnS/MMT/g-C_3N_4.

pseudo-second-order model can describe the Rh. B adsorption on the ZnS/MMT/g-C_3N_4; higher value of correlation coefficient explains this subject.

Photocatalyst Activity

To determine the photocatalyst activity of ZnS/MMT/g-C_3N_4, the degradation of Rh. B was evaluated under optimum condition including dark, LED, and UV irradiations. Based on the data, the percentage of Rh. B removal was 93% under UV irradiations as the best condition, and the trapping experiment demonstrated the effect of radicals.

Mechanism of Rh. B Removal

For the removal of Rh. B, the adsorption and photocatalytic activities were evaluated by ZnS/MMT/g-C_3N_4 composite. In the adsorption process, the Rh. B was removed to the surface of ZnS/MMT/g-C_3N_4 composite, and it got into the as-prepared composite, due to the hydrogen bonding and electrostatic (π-π) interactions. In the photocatalytic process, the irradiations were absorbed by ZnS/MMT/g-C_3N_4 composite, and the electron-hole pairs

were generated by MMT/g-C_3N_4. Then, the electrons in the conduction band (CB) of MMT/g-C_3N_4 were injected into the CB of ZnS, and the holes in valence band (VB) of ZnS could be migrated to the VB of the MMT/g-C_3N_4. The hydroxyl and superoxide radicals can be attacked for the degradation of Rh. B (Scheme 1) [39,40].

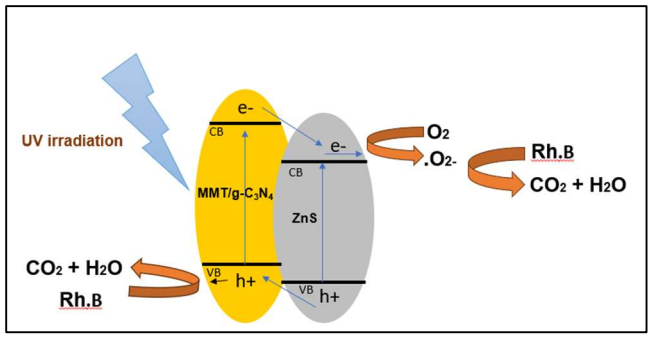

Scheme 1. Proposed mechanism for Rh.B removal by ZnS/MMT/g-C_3N_4 composite

Comparison of Different Materials for the Removal of Rh. B

Table 4 shows the yield of Rh. B removal by several compounds; some of these adsorbents only showed the adsorbent property, but the inability for the Rh. B degradation was obvious. In some literature reports, the interaction of some parameters hasn't been investigated. In many photocatalysts, adding the semiconductor led to a decrease in surface area, but the surface area was increased in the as-synthesized composite. Furthermore, the ZnS/MMT/g-C_3N_4 composite showed a better adsorption compared to that of MT.

Several composites have been used for the degradation of organic pollutant and pigments. According to Table 5, ternary or multicomponent composite can be acted more efficient compared to a binary component system, due to the efficient separation of the charge carriers [3]. More negative CB and valence band VB can lead to a better yield and useful heterostructure composite. The efficient charge transfer was obtained in the g-C_3N_4-based type II and Z-Scheme heterostructures. The ZnS/MMT/g-C_3N_4 is trinary heterostructure composite forming by using natural composite, and suitable charge transfer can provide more advantages for this composite compared to other composites (Entries 1-8). Furthermore, the more specific area compared to some other photocatalysts is an advantage of this as-synthesized composite.

CONCLUSIONS

The goal of this study was studying the combination of adsorbent and photocatalytic activity for the pollution removal; hence, the ZnS/MMT/g-C_3N_4 was synthesized by a simple procedure. Adding MMT to ZnS resulted in an increase in the surface area and the efficiency of charge transfer. Response surface methodology (RSM) was employed for the predication of the best model for the Rh. B removal. The pH and ZnS/MMT/g-C_3N_4 dosage were shown as important factors affecting the Rh. B. removal.

Table 4. Comparation of Adsorbent Activity for the Rh. B Removal

Entry	Materials	Yeild (%)	Ref.
1	MonoBODIPY-functionalized Fe_3O_4@SiO_2@TiO_2 nanoparticles	29.49	[41]
2	PVDF/g-C_3N_4/chitosan	72.74	[42]
3	Reduced graphene-nickel nanocomposite	90	[43]
4	Reduced graphene oxide	98	[44]
5	TiO_2 nanofibers membrane loaded on porous fly ash ceramic support	97.74	[45]
6	$ZnFe_2O_4$ and UiO-66 over g-C_3N_4		[46]
7	MMT	81	This work
8	ZnS/MMT/g-C_3N_4	93	This work

Table 5. Typical g-C_3N_4-based Heterojunction Photocatalysts

Entry	Photocatalysts	Application	Charge transfer type	Ref.
1	TiO_2/g-C_3N_4	MB photodegradation	Type II heterojunction photocatalysts	[47]
2	ZnO/g-C_3N_4	Rhodamine B photodegradation	Type II heterojunction photocatalysts	[48]
3	CdS/g-C_3N_4	MB photodegradation	Type II heterojunction photocatalysts	[49]
4	MoS_2/g-C_3N_4	MO photodegradation	Type II heterojunction photocatalysts	[50]
5	Bi_2WO_6/RGO/g-C_3N_4	2,4,6-Trichlorophenol (TCP) photodegradation	Z-scheme	[51]
6	Fe_2O_3/g-C_3N_4	RhB photodegradation	Direct Z-scheme	[52]
7	WO_3/g-C_3N_4	MB photodegradation	Direct Z-scheme	[53,54]
8	Ag_2WO_4/g-C_3N_4	MO photodegradation	Direct Z-scheme	[55]

The optimum condition for the adsorption were obtained at the pH of 5.5, 0.05 g ZnS/MMT/g-C_3N_4, and 5 ppm Rh. B. The degradation of Rh. B reached 93% under UV irradiation. The synthesis of ZnS/MMT/g-C_3N_4 led to the design of a novel material with the adsorption and photocatalytic synergic role. These challenges can be addressed in the future research works: (1) The optimization of composite amounts. (2) More detailed analysis on the mechanism of photocatalyst. (3) The ability of the composite for the removal of other organic materials. (4) Theoretical calculation to determine the thermodynamic and kinetic status of reaction. (5) Considering the effective parameter for photolysis reaction.

REFERENCES

[1] Kong, L.; Wang, J.; Ma, F.; Sun, M.; Quan, J., Graphitic carbon nitride nanostructures: Catalysis. *Appl. Mater. Today.* **2019**, *16*, 388-424, DOI: 10.1016/ j.apmt.2019.06.003.

[2] Magesa, F.; Wu, Y.; Tian, Y.; Vianney, J.-M.; Buza, J.; He, Q.; Tan, Y., Graphene and graphene like 2D graphitic carbon nitride: Electrochemical detection of food colorants and toxic substances in environment. *Trends Environ. Anal. Chem.* **2019**, *23*, e00064, DOI: 10.1016/j.teac.2019.e00064.

[3] Fu, J.; Yu, J.; Jiang, C.; Cheng, B., g-C_3N_4-Based heterostructured photocatalysts. *Adv. Energy Mater.* **2018**, *8 (3)*, 1701503, DOI: 10.1002/aenm.201701503.

[4] Ren, X.; Zhang, Y.; Yang, L.; Chen, Z., Degradation of ofloxacin by peroxymonosulfate activated with cobalt-doped graphitic carbon nitride: Mechanism and performance. *Inorg. Chem. Commun.* **2021**, *133*, 108863 DOI: 10.1016/j.inoche.2021.108863.

[5] Saravanan, V.; Lakshmanan, P.; Ramalingan, C., Alumina surface modified with graphitic carbon nitride: Synthesis, characterization and its application as photocatalyst. *Diam. Relat.* **2021**, *114*, 108291, DOI: 10.1016/j.diamond.2021.108291.

[6] Mohammad, A.; Khan, M. E.; Cho, M. H.; Yoon, T., Graphitic-carbon nitride based mixed-phase bismuth nanostructures: Tuned optical and structural properties with boosted photocatalytic performance for wastewater decontamination under visible-light irradiation. *NanoImpact,* **2021**, *23*, 100345, DOI: 10.1016/j.impact.2021.100345.

[7] Xu, L.; Li, L.; Fang, P.; Chang, K.; Chen, C.; Liao, Q., Removal of uranium (VI) ions from aqueous solution by graphitic carbon nitride stabilized FeS nanoparticles. *J. Mol. Liq.* **2021**, *117050*, DOI: 10.1016/ j.molliq.2021.117050.

[8] Li, R.; Ma, H.; Shu, J.; Lian, Z.; Chen, N.; Ou, S.; Jin, R.; Li, S.; Yang, H., Surface engineering of copper sulfide-titania-graphitic carbon nitride ternary

nanohybrid as an efficient visible-light photocatalyst for pollutant photodegradation. *J. Mol. Liq.* **2021**, *604*, 198-207, DOI: 10.1016/j.molliq.2021.117050.

[9] Wang, S.; Chen, L.; Zhao, X.; Zhang, J.; Ao, Z.; Liu, W.; Wu, H.; Shi, L.; Yin, Y.; Xu, X.; Zhao, C.; Duan, X.; Wang, S.; Sun, H., Efficient photocatalytic overall water splitting on metal-free 1D SWCNT/2D ultrathin C_3N_4 heterojunctions via novel non-resonant plasmonic effect. *Appl. Catal. B: Environ.* **2020**, *278*, 119312, DOI: 10.1016/j.apcatb.2020.119312.

[10] Sun, Z.; Li, C.; Du, X.; Zheng, S.; Wang, G., Facile synthesis of two clay minerals supported graphitic carbon nitride composites as highly efficient visible-light-driven photocatalysts. *J. Colloid Interface Sci.* **2018**, *511*, 268-276, DOI: 10.1016/j.jcis.2021.07.030.

[11] Zhang, C.; Li, Y.; Shuai, D.; Zhang, W.; Niu, L.; Wang, L.; Zhang, H., Visible-light-driven, water-surface-floating antimicrobials developed from graphitic carbon nitride and expanded perlite for water disinfection. *Chemosphere* **2018,** *208*, 84-92, DOI: 10.1016/j.chemosphere.2018.05.163.

[12] Chegeni, M.; Mehri, M.; Dehdashtian, S., Photocatalytic bauxite and red mud/graphitic carbon nitride composites for Rhodamine B removal. *J. Mol. Struct.* **2021**, *1242*, 130752, DOI: 10.1016/j.molstruc.2021.130752.

[13] Hao, Q.; Chen, T.; Wang, R.; Feng, J.; Chen, D.; Yao, W., A separation-free polyacrylamide/bentonite/graphitic carbon nitride hydrogel with excellent performance in water treatment. *J. Clean. Prod.* **2018**, *197*, 1222-1230, DOI: 10.1016/j.jclepro.2018.06.289.

[14] Shetti, N. P.; Nayak, D. S.; Reddy, K. R.; Aminabhvi, T. M., *Graphene-Clay-Based Hybrid Nanostructures for Electrochemical Sensors and Biosensors.* In *Graphene-Based Electrochemical Sensors for Biomolecules*, Elsevier: **2019**, pp. 235-274.

[15] Zhang, H.; Zhu, C.; Wei, C.; Duan, H.; Yu, J., *Application of functionalized nanomaterials in asphalt road construction materials.* In *Handbook of Functionalized Nanomaterials for Industrial Applications*, Elsevier: **2020**, pp. 865-907.

[16] Zhou, C.; Tong, D.; Yu, W., *Smectite Nanomaterials: Preparation, Properties, and Functional Applications. In Nanomaterials from Clay Minerals*, Elsevier: **2019**, pp. 335-364.

[17] Duleba, B.; Greškovič, F.; Spišák, E.; Dulebová, Ľ., Preparation and Characterization of Polypropylene/MMT Nanocomposites. *Adv. Mater. Res.* **2014**, *893*, 132-135.

[18] Devi, S. H. K.; Shashidhara, G. M.; Ghosh, A. K., Characterization of HDPE/MMT-Based Nanocomposites. *Composite Interfaces* **2010**, *17* (2-3), 217-222,DOI: 4028/www.scientific.net/AMR.893.132.

[19] Peng, K.; Wang, H.; Li, X.; Wang, J.; Cai, Z.; Su, L.; Fan, X., Emerging WS_2/montmorillonite composite nanosheets as an efficient hydrophilic photocatalyst for aqueous phase reactions. *Sci. Rep.* **2019**, *9* (1), 16325, DOI: 10.1038/s41598-019-52191-9.

[20] Rhee, C. H.; Kim, H. K.; Chang, H.; Lee, J. S., Nafion/Sulfonated Montmorillonite Composite: A New Concept Electrolyte Membrane for Direct Methanol Fuel Cells. *Chem. Mater.* **2005**, *17* (7), 1691-1697, DOI: 10.1021/cm048058q.

[21] Li, X.; Peng, K., $MoSe_2$/Montmorillonite Composite Nanosheets: Hydrothermal Synthesis, Structural Characteristics, and Enhanced Photocatalytic Activity. *Minerals* **2018**, *8* (7), 268, DOI: 10.3390/min8070268.

[22] Yoon, J.; Kim, I. T.; Bae, J.; Hur, J., High-performance ZnS@graphite composites prepared through scalable high-energy ball milling as novel anodes in lithium-ion batteries. *J. Ind. Eng. Chem.* **2019**, *76*, 258-267, DOI: 10.1016/j.jiec.2019.03.050.

[23] Ikkurthi, K. D.; Srinivasa Rao, S.; Ahn, J. -W.; Sunesh, C. D.; Kim, H. -J., A cabbage leaf like nanostructure of a NiS@ZnS composite on Ni foam with excellent electrochemical performance for supercapacitors. *Dalton trans.* **2019,** *48 (2)*, 578-586, DOI: 10.1039/C8DT04139C.

[24] Zhang, X.; Liu, X.; Zhang, L.; Li, D.; Liu, S., Novel porous Ag_2S/ZnS composite nanospheres: fabrication and enhanced visible-light photocatalytic activities. *J. Alloys Compd.* **2016**, *655*, 38-43, DOI: 10.1016/j.jallcom.2015.08.202.

[25] Chang, C. -J.; Huang, K. -L.; Chen, J. -K.; Chu, K. -W.; Hsu, M. -H., Improved photocatalytic hydrogen production of ZnO/ZnS based photocatalysts by Ce doping. *J. Taiwan Inst. Chem.* **2015**, *55*, 82-89, DOI: 10.1016/j.jtice.2015.04.024.

[26] Ojovan, M. I.; Lee, W. E.; Kalmykov, S. N., *Treatment of Radioactive Wastes.* In *An Introduction to Nuclear Waste Immobilisation (Third Edition)*, Elsevier: **2019**;, p. 231-269.

[27] Agarwal, S.; Tyagi, I.; Gupta, V. K.; Dehghani, M. H.; Ghanbari, R., Investigating the residual aluminum elimination from conventional and enhanced coagulation by phosphate compounds in wastewater treatment process. *J. Mol. Liq.* **2016**, *221*, 673-684, DOI: 10.1016/j.molliq.2016.06.051.

[28] Jin, Y. -Z.; Zhang, Y. F.; Li, W., Micro-electrolysis technology for industrial wastewater treatment. *J. Environ. Sci.* **2003**, *15*, 334-338, DOI: 12938982.

[29] Bartels, C. R.; Wilf, M.; Andes, K.; Iong, J., Design considerations for wastewater treatment by reverse osmosis. *Water Sci. Technol.* **2005**, *51* (6-7), 473-482, DOI: 10.2166/wst.2005.0670.

[30] Eom, T. -H.; Lee, C. -H.; Kim, J. -H.; Lee, C. -H., Development of an ion exchange system for plating wastewater treatment. *Desalination* **2005**, *180* (1), 163-172, DOI: 10.1016/j.desal.2004.11.088.

[31] Chai, W. S.; Cheun, J. Y.; Kumar, P. S.; Mubashir, M.; Majeed, Z.; Banat, F.; Ho, S. -H.; Show, P. L., A review on conventional and novel materials towards heavy metal adsorption in wastewater treatment application. *J. Clean. Prod.* **2021**, *296*, 126589, DOI: 10.1016/j.jclepro.2021.126589.

[32] Mohammadi, R.; Tang, W.; Sillanpää, M., A systematic review and statistical analysis of nutrient recovery from municipal wastewater by electrodialysis. *Desalination* **2021**, *498*, 114626, DOI: 10.1016/j.desal.2020.114626.

[33] Cheng, D.; Liu, Y.; Ngo, H. H.; Guo, W.; Chang, S. W.; Nguyen, D. D.; Zhang, S.; Luo, G.; Liu, Y., A review on application of enzymatic bioprocesses in animal wastewater and manure treatment. *Bioresour. Technol.* **2020**, *313*, 123683, DOI: 10.1016/j.biortech.2020.123683.

[34] Singla, A., Review of biological treatment solutions and role of nanoparticles in the treatment of wastewater generated by diverse industries. *Nanotechnol. Environ. Eng.* **2022**, *7* (3), 699-711, DOI: 10.1007/s41204-022-00267-9.

[35] Nasir, A. M.; Jaafar, J.; Aziz, F.; Yusof, N.; Salleh, W. N. W.; Ismail, A. F.; Aziz, M., A review on floating nanocomposite photocatalyst: Fabrication and applications for wastewater treatment. *JWPE,* **2020**, *36*, 101300, DOI: 10.1016/j.jwpe.2020.101300.

[36] Wang, Q.; Zhang, B.; Lu, X.; Zhang, X.; Zhu, H.; Li, B., Multifunctional 3D $K_2Ti_6O_{13}$ nanobelt-built architectures towards wastewater remediation: selective adsorption, photodegradation, mechanism insight and photoelectrochemical investigation. *Catal. Sci. Technol.* **2018**, *8* (23), 6180-6195, DOI: 10.1039/C8CY01684D.

[37] Richardson, S. D.; Willson, C. S.; Rusch, K. A., Use of Rhodamine water tracer in the marshland upwelling system. *Ground Water,* **2004**, *42* (5), 678-88, DOI: 10.1111/j.1745-6584.2004.tb02722.x.

[38] Sano, T.; Koike, K.; Hori, T.; Hirakawa, T.; Ohko, Y.; Takeuchi, K., Removal of methyl mercaptan with highly-mobile silver on graphitic carbon-nitride (g-C_3N_4) photocatalyst. *Appl. Catal. B.* **2016**, *198*, 133-141, DOI: 10.1016/j.apcatb.2016.05.057.

[39] Wang, Q.; Xu, P.; Zhang, G.; Hu, L.; Wang, P., Visible-light responsive g-C_3N_4 coupled with ZnS nanoparticles via a rapid microwave route: Characterization and enhanced photocatalytic activity. *Appl. Surf. Sci.* **2019**, *488*, 360-369, DOI: 10.1016/j.apsusc.2019.05.238.

[40] Xu, J.; Qi, Y.; Wang, W.; Wang, L., Montmorillonite-hybridized g-C_3N_4 composite modified by NiCoP cocatalyst for efficient visible-light-driven photocatalytic hydrogen evolution by dye-sensitization. *Int. J. Hydrog.* **2019**, *44* (8), 4114-4122, DOI: 10.1016/j.ijhydene.2018.12.167.

[41] Bilgic, A., Fabrication of monoBODIPY-functionalized Fe_3O_4@SiO_2@TiO_2 nanoparticles for the photocatalytic degradation of rhodamine B under UV irradiation and the detection and removal of Cu(II) ions in aqueous solutions. *J. Alloys Compd.* **2022**, *899*, 163360, DOI: 10.1016/j.jallcom.2021.163360.

[42] Gharbani, P.; Mehrizad, A., Preparation and characterization of graphitic carbon nitrides/polyvinylidene fluoride adsorptive membrane modified with chitosan for Rhodamine B dye removal from water: Adsorption isotherms, kinetics and thermodynamics. *Carbohydr. Polym.* **2022**, *277*, 118860, DOI: 10.1016/j.carbpol.2021.118860.

[43] Jinendra, U.; Bilehal, D.; Nagabhushana, B. M.; Kumar,

A. P., Adsorptive removal of Rhodamine B dye from aqueous solution by using graphene-based nickel nanocomposite. *Heliyon* **2021**, *7* (4), e06851, DOI: 10.1016/j.heliyon.2021.e06851.

[44] Parvathi, E.; Arjun, G.; Akshaya, C. V.; Dilraj, N.; Deepak, N. K., Novel Mussaenda glabrata leaves extract for facile green synthesis of reduced graphene oxide with enhanced Rhodamine B dye removal efficiency. *Sustain. Chem. Pharm.* **2022**, *30*, 100868, DOI: 10.1016/j.scp.2022.100868.

[45] Abdelaal, K.; Essawy, M.; Quraytam, A.; Abdallah, F.; Mostafa, H.; Shoueir, K.; Fouad, H.; Hassan, F. A. S.; Hafez, Y., Toxicity of Essential Oils Nanoemulsion Against Aphis Craccivora and Their Inhibitory Activity on Insect Enzymes. *Processes* **2021**, *9*, DOI: 10.3390/pr9040624.

[46] Sharafinia, S.; Farrokhnia, A.; Lemraski, E. G.; Rashidi, A., Decoration of $ZnFe_2O_4$ and UiO-66 over g-C_3N_4 as magnetically novel reusable visible light photocatalyst for degradation of Rh–B. *Opt. Mater.* **2022**, *132*, 112838, DOI: 10.1016/j.optmat.2022.112838.

[47] Xia, P.; Zhu, B.; Yu, J.; Cao, S.; Jaroniec, M., Ultra-thin nanosheet assemblies of graphitic carbon nitride for enhanced photocatalytic CO_2 reduction. *J. Mater. Chem.* **2017**, *5* (7), 3230-3238, DOI: 10.1039/C6TA08310B.

[48] Wang, Y.; Shi, R.; Lin, J.; Zhu, Y., Enhancement of photocurrent and photocatalytic activity of ZnO hybridized with graphite-like C_3N_4. *Energy Environ. Sci.* **2011**, *4* (8), 2922-2929, DOI: 10.1039/C0EE00825G.

[49] Jiang, F.; Yan, T.; Chen, H.; Sun, A.; Xu, C.; Wang, X., A g-C_3N_4–CdS composite catalyst with high visible-light-driven catalytic activity and photostability for methylene blue degradation. *Appl. Surf. Sci.* **2014**, *295*, 164-172, DOI: 10.1016/j.apsusc.2014.01.022.

[50] Peng, W. -C.; Li, X. -Y., Synthesis of MoS_2/g-C_3N_4 as a solar light-responsive photocatalyst for organic degradation. *Catal. Commun.* **2014**, *49*, 63-67, DOI: 10.1016/j.catcom.2014.02.008.

[51] Ma, D.; Wu, J.; Gao, M.; Xin, Y.; Ma, T.; Sun, Y., Fabrication of Z-scheme g-C_3N_4/RGO/Bi_2WO_6 photocatalyst with enhanced visible-light photocatalytic activity. *J. Chem. Eng.* **2016**, *290*, 136-146, DOI: 10.1016/j.cej.2016.01.031.

[52] Wang, J.; Li, C.; Cong, J.; Liu, Z.; Zhang, H.; Liang, M.; Gao, J.; Wang, S.; Yao, J., Facile synthesis of nanorod-type graphitic carbon nitride/Fe_2O_3 composite with enhanced photocatalytic performance. *J. Solid State Chem.* **2016**, *238*, 246-251, DOI: 10.1016/j.jssc.2016.03.042.

[53] Chen, S.; Hu, Y.; Meng, S.; Fu, X., Study on the separation mechanisms of photogenerated electrons and holes for composite photocatalysts g-C_3N_4-WO_3. *Appl. Catal.* **2014**, *150*, 564-573, DOI: 10.1016/j.apcatb.2013.12.053.

[54] Cui, L.; Ding, X.; Wang, Y.; Shi, H.; Huang, L.; Zuo, Y.; Kang, S., Facile preparation of Z-scheme WO_3/g-C_3N_4 composite photocatalyst with enhanced photocatalytic performance under visible light. *Appl. Surf. Sci.* **2017**, *391*, 202-210, DOI: 10.1016/j.apsusc.2016.07.055.

[55] Zhu, B.; Xia, P.; Li, Y.; Ho, W.; Yu, J., Fabrication and photocatalytic activity enhanced mechanism of direct Z-scheme g-C_3N_4/Ag_2WO_4 photocatalyst. *Appl. Surf. Sci.* **2017**, *391*, 175-183, DOI: 10.1016/j.apsusc.2016.07.104.